FaIR v2.0: a generalised impulse-response model for climate uncertainty and future scenario exploration, integrated assessment, and teaching

Nicholas J. Leach[1⋆]
Stuart Jenkins[1]
John Lynch[1]
Michelle Cain[1]
Junichi Tsutsui[2]
Christopher Smith[3]
Zebedee Nicholls[4]
Myles R. Allen[1,5]

[1]Department of Physics, Atmospheric Oceanic and Planetary Physics, University of Oxford, United Kingdom.
[2]Environmental Science Laboratory, Central Research Institute of Electric Power Industry, Abiko-shi, Japan.
[3]School of Earth and Environment, University of Leeds, Leeds, UK.
[4]Australian–German Climate and Energy College, University of Melbourne, Australia
[5]Environmental Change Institute, University of Oxford, Oxford, UK.
⋆contact email: Nicholas.leach@stx.ox.ac.uk

Abstract

Here we present a new simple climate model for use in probabilistic future climate and scenario exploration, integrated assessment, policy and teaching. This model is based on a set of only six equations, but includes physically-motivated state-dependent feedbacks on the response timescales of each simulated gas cycle. These six equations are simple and transparent enough to be easily understood and used in teaching, but flexible enough to be able to accurately (with respect to the observational record) model key climate variables such as well-mixed greenhouse gas (GHG) concentrations and atmospheric lifetimes, effective radiative forcing, and forced temperature anomaly. We describe the assumptions and methods used in selecting the default parameters, but emphasize that other methods would be equally valid, and could lead to alternative model output. The tunable nature of the model lends it to use as an emulator of high complexity Earth System Models, such as those participating in CMIP6, and allows the properties of these complex models to be investigated compared more simply. The model design is such that it can be written in tabular data analysis software, such as Excel, increasing the potential user base of the model considerably.

1 Introduction

Earth System Models (ESMs) are vital tools for providing insight into the drivers behind Earths climate system, as well as predicting impacts of future emissions. Large scale multi-model studies, such as the Coupled Model Intercomparison Project (CMIP), have been used in many reports to produce projections of what the future climate may look like based on a range of different emissions scenarios and associated socio-economic narratives provided by Integrated Assessment Models (IAMs). In addition

to simulating both the past and possible future climates, these CMIPs extensively use theoretical experiments to try to constrain some of the key properties of the climate system, such as the equilibrium climate sensitivity [ECS, Collins et al. (2013)], or the transient climate response to cumulative carbon emissions [TCRE, Allen et al. (2009)]. While ESMs are integral to our current best understanding of the how the climate system responds to GHG emissions, and provide the current best predictions for what a future world might look like, they are so computationally expensive that we are only able to run a limited set of experiments during a CMIP. This constraint on the quantity of experiments and scenarios able to be simulated necessitates the use of simpler emulators to provide probabilistic assessments and explore additional experiments and scenarios. These emulators are often referred to as simple climate models (SCMs). In general, they are able to simulate the globally averaged emission $\rightarrow$ concentration $\rightarrow$ radiative forcing $\rightarrow$ temperature response pathway, and can be tuned to emulate an individual ESM (or multi-model-mean). In terms of complexity, SCMs are considerably lighter than ESMs, both in terms of the runtime (most SCMs can run thousands of years of simulation per minute on an "average" personal computer, whereas ESMs take several hours to run a single year on a supercomputer), and the number of lines of code (SCMs tend to be composed of the order of thousands, whereas ESMs are of the order of millions of lines).

Several simple climate models are available, such as the two used in the Intergovernmental Panel on Climate Change (IPCC) Special Report on 1.5°C warming (IPCC, 2018, SR15): FaIR v1.3 and MAGICC6. However, while these models are "simple" in comparison to the ESMs they emulate, they are often still not so simple as to allow new users to quickly and easily understand the equations and processes behind their calculations. This learning curve behind the use of these simple models reduces their usability, and has meant that different research groups tend to use the model they are most familiar with. This has led to a number of different simple climate models being used in single reports for identical tasks, reducing the overall consistency of the work. We believe one key step towards a transparent and coherent process in reports such as SR15 is the use of a single SCM between working groups, and would allow results to be directly comparable throughout. Such a model would be a "lowest common denominator" model within these reports.

In this paper, we introduce a simple, transparent, and flexible climate model based on FaIR v1.0 (Millar et al., 2017) that uses four equations to model the atmospheric cycles and corresponding effective radiative forcing (ERF) impact of three major greenhouse gases, and a further two to emulate the climate system's thermal response to changes in ERF; these are outlined in figure 1. Despite their simplicity, these equations do still represent physical process and the model is therefore not an entirely abstracted emulator with no basis in the real world. We describe the methods behind selecting a default parameter set and associated uncertainties for the model using some constraints from more complex models and existing literature, but ultimately chosen to accurately represent historical observations. We demonstrate that this parameter set can closely replicate inferred properties of the climate system in both historical observations and more complex models. We compare the models response with other widely used simple climate models for a subset of the Shared Socioeconomic Pathways ,(Riahi et al., 2017, SSPs), all using their respective default parameter sets. Previous work (Joos et al., 2013; Tsutsui, 2017) indicates that the model parameters can be adjusted to emulate the behaviour of ESMs, suggesting that our model could act as a probabilistic emulator for individual CMIP6 ESMs, something we aim to demonstrate when sufficient CMIP6 output is available.

The model is sufficiently simple as to be able to be used (and crucially understood) in undergraduate and high-school teaching of climate change, and can illustrate some key properties of the climate system such as the very different warming impacts of different GHGs, or the widely discussed equilibrium climate sensitivity. To allow students and other users unfamilliar with scientific programming

languages (such as the model's native language, python) access to the model, we also provide a version of the model written in Excel. We hope that this may open exploration of the climate system to a large group of potential users who do not have the expertise to run presently-available available SCMs. The simplicity of the model additionally means that although we provide code for the model, users do not need to rely on this, and would be able to relatively quickly re-create the model in whatever language they are familiar with, and whatever format fits their intended usage. This increases the potential of the model for use in integrated assessment, as instead of having to adapt existing code to run within an existing architecture, new code for this model could be written in exactly the format and structure required.

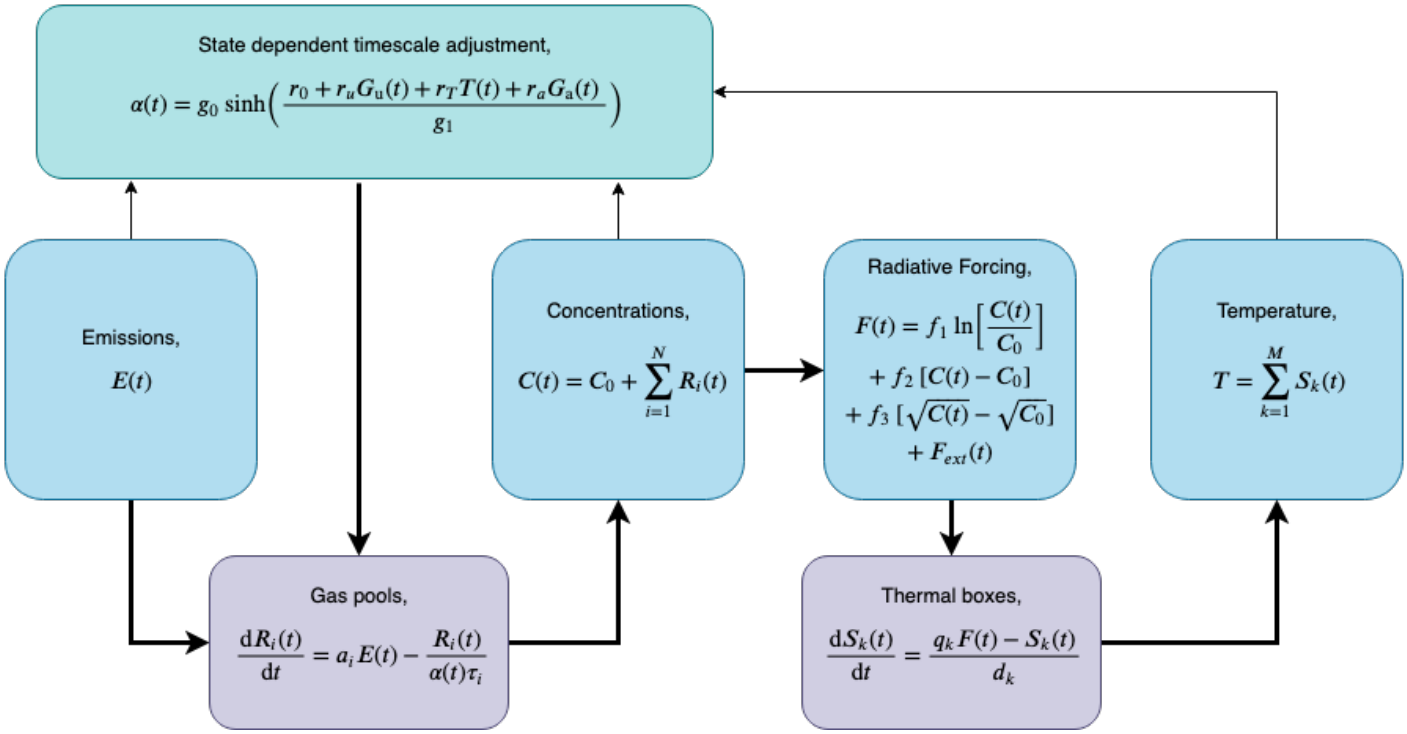

Figure 1: Schematic showing the full model structure and equations used. Model steps take place from left to right, with thick arrows indicating steps that occur during timestep t, and thin arrows indicating steps that occur in between timesteps t and $t + dt$. Equations are described in full below.

2 Emissions to concentrations

Model description

FaIR v2.0 models the relationship between emissions and atmospheric concentrations of a gas species (the gas cycle) with three equations:

$$\frac{\mathrm{d}R_i(t)}{\mathrm{d}t} = a_i E(t) - \frac{R_i(t)}{\alpha\tau_i}, \tag{1}$$

$$C(t) = C_0 + \sum_{i=1}^{n} R_i(t) \quad \text{and} \tag{2}$$

$$\alpha(t) = g_0 \cdot \sinh\Big(\frac{r_0 + r_u G_u(t) + r_T T(t) + r_a G_a(t)}{g_1}\Big); \tag{3}$$

$$\text{where} \quad g_1 = \sum_{i=1}^{4} a_i\tau_i\big[1 - \big(1 + h/\tau_i\big)\mathrm{e}^{-h/\tau_i}\big]$$

$$\text{and} \quad g_0 = \Big[\sinh\Big(\frac{\sum_{i=0}^{3} a_i\tau_i[1 - \mathrm{e}^{-h/\tau_i}]}{g_1}\Big)\Big]^{-1}.$$

Equations 1 and 2 describe a gas cycle with an atmospheric burden above the pre-industrial concentration, C_0, formed of n pools: each pool corresponds to a different sink from the atmosphere. Each pool, R_i, has an uptake fraction a_i and decay timescale τ_i, which is multiplicatively adjusted by a state dependent factor, α. At each timestep, time t, α is computed, and then the pool concentrations are updated and summed to determine the new atmospheric burden. α provides feedbacks to the gas lifetimes based on the current timestep levels of accumulated gas, temperature, and atmospheric gas burden, encapsulated by the r coefficients. The form of α, 3, is an analytic approximation to the numerical solution of the 100-year integrated Impulse Response Function (iIRF100) from equations 7 and 8 in Millar et al. (2017). We include possible state dependencies on the cumulative carbon uptake mass, G_u, the temperature, T, and an additional term not in FaIR v1.3 dependent on $G_a(t)$, the atmospheric mass burden, motivated by the sensitivities of the CH_4 and N_2O lifetimes to their own abundances as predicted by atmospheric chemistry and simulated in chemical transport models (CTMs) (Holmes et al., 2013; Prather et al., 2015). g_0 and g_1 set the value and gradient of our analytic approximation equal to the numerical solution at $\alpha = 1$. We discuss the suitability of this analytic form in the Supplementary Information and compare it to the numerical solution used in FaIR v1.3 (Smith et al., 2017). While we do not include any lifetime feedbacks beyond those described above to avoid having to specify additional exogenous variables, such as NOx feedback on the CH_4 lifetime, these could theoretically be incorporated in the same framework by adding r coefficients to the model.

Observationally consistent parameter selection

Here we discuss default parameter choices for the three greenhouse gases (GHGs) that have contributed the most to global warming since pre-industrial times: carbon dioxide (CO_2), methane (CH_4) and nitrous oxide (N_2O). The CO_2 gas cycle is highly similar to those in FaIR v1.0 (Millar et al., 2017) and FaIR v1.3 (Smith et al., 2017): a four carbon pool cycle with a decay timescale dependence on G_u and T. The CH_4 gas cycle has a single pool, with lifetime state dependencies on T and G_a. While in reality, CH_4 has several sinks (tropospheric OH, tropospheric Cl, stratospheric reactions and soil uptake) and a lifetime dependent on many more variables (Holmes et al., 2013), we find that our model is sufficient for reproducing observed emission to concentration pathways. The N_2O gas cycle has a single pool and a lifetime dependent only on G_a.

For CO_2 we keep values of a_i and τ_i identical to those in FaIR v1.0 and v1.3 (Millar et al., 2017; Smith et al., 2017), originally from Myhre et al. (2013). r_0, r_u and r_T are tuned to reproduce present day concentrations – from the CMIP6 historical concentrations dataset, extended to 2017 with up-to-date measurements from NOAA (Meinshausen et al., 2017; Battle et al., 1996; Butler et al., 1999) – when the model is spun up from pre-industrial with bottom-up emission estimates from the Global Carbon Project (Quéré et al., 2018) and run with a prescribed temperature pathway of attributable warming to the present day [calculated as described in Haustein et al. (2017) using best-estimate forcings based on Forster et al. (2013) and the mean of four temperature datasets (Vose et al., 2012; Cowtan and Way, 2014; Lenssen et al., 2019; Morice et al., 2011)], fixing the ratio of r_u and r_T to the FaIR v1.0 and v1.3 default. Uncertainties in r_0, r_u and r_T are taken from Millar et al. (2017).

The CH_4 gas cycle only has a single pool, so a_i is zero except for $i = 1$. We set τ_1 to the present-day lifetime found in Holmes et al. (2013). We fit r_T and r_a to the sensitivities of the CH_4 lifetime to tropospheric air temperature, tropospheric water vapour and CH_4 abundance in Holmes et al. (2013) by linearising FaIR v2.0 and the parametric model in Holmes et al. about 2010 variable values. We find that a global mean temperature dependence is sufficient to reproduce the sensitivities to both tropospheric air temperature and water vapour due to the close thermodynamic relationship between these quantities. We then fit the specified pre-industrial concentration and r_0 in an identical model run to the CO_2 parameter fitting procedure, but using bottom-up emission estimates from PRIMAP-histTP (Gütschow et al., 2016). While the parametric model in Holmes et al. includes lifetime sensitivities to eight other atmospheric variables such as anthropogenic NOx emissions, many of these have a small effect and all are scenario-dependent, requiring additional exogenous variables to be specified. Since we wish each gas cycle model to be independent we do not include any more state dependencies in addition to those described above. Uncertainties in τ_1, r_T and r_a are derived from the uncertainties given in Holmes et al. (2013). We recommend that when using a Transient Climate Reponse (TCR) thermal parameter value that differs from the central estimate of 1.58K, both the CO_2 and CH_4 r_T parameter values be scaled to match the ratio of the chosen TCR to the central estimate.

The N_2O gas cycle only has a single pool, so a_i is zero except for $i = 1$. We set τ_1 to the present-day lifetime found in Prather et al. (2015). We fit r_a to the sensitivity of the N_2O lifetime to its own burden found in Prather et al. (2015) by linearising FaIR v2.0 and the parametric model in Prather et al. about 2010 variable values. We then fit the specified pre-industrial concentration and r_0 as for CH_4. All other variables that affect the N_2O lifetime in Prather et al. are discarded to keep the gas cycle model independent as with CH_4. Uncertainties in τ_1 and r_a are derived from the uncertainties given in Prather et al. (2015).

The resulting tuned default parameters are given below, alongside their values in FaIR v1.0 and v1.3. Note that FaIR v1.3 has effective parameter values of r_u, r_T, $r_a = 0$ and a value of r_0 set such that $\alpha = 1$, and that FaIR v1.0 does not include CH_4 or N_2O. We emphasize that many choices have been made in selecting these parameters and different choices would lead to potentially quite different parameter values. One example of this is given in parentheses, in which we fit the CH_4 r_0 parameter by tuning inverse emissions from FaIR v2.0 to the best-estimate top-down anthropogenic emission estimate in the recent Global Methane Budget (Saunois et al., 2019), while setting the pre-industrial concentration to the 1500-1800 mean of 720 ppb from Meinshausen et al. (2017).

Table 1: Default parameter values for the gas cycle components in different versions of FaIR. Where relevant, uncertainties for FaIR v2.0 are included as the 1-σ range and are assumed to be normally distributed.

Parameter	FaIR v2.0			FaIR v1.3			FaIR v1.0		
	CO_2	CH_4	N_2O	CO_2	CH_4	N_2O	CO_2	CH_4	N_2O
a_1	0.2173	1	1	0.2173	1	1	0.2173	-	-
a_2	0.2240	0	0	0.2240	0	0	0.2240	-	-
a_3	0.2824	0	0	0.2824	0	0	0.2824	-	-
a_4	0.2763	0	0	0.2763	0	0	0.2763	-	-
τ_1	1000000	$9.15 \pm 10\%$	$116 \pm 8\%$	1000000	9.3	121	1000000	-	-
τ_2	394.4	-	-	394.4	-	-	394.4	-	-
τ_3	36.54	-	-	36.54	-	-	36.54	-	-
τ_4	4.304	-	-	4.304	-	-	4.304	-	-
r_0	$28.63 \pm 8\%$	9.079 (8.445)	67.84	35.0	-	-	32.4	-	-
r_u	$0.01977 \pm 8\%$	0	0	0.019	-	-	0.019	-	-
r_T	$4.334 \pm 8\%$	$-0.2872 \pm 15\%$	0	4.165	-	-	4.165	-	-
r_a	0	$0.0003434 \pm 13\%$	$-0.0009993 \pm 16\%$	0	-	-	0	-	-
C_0	278	733.8 (720.0)	271.26	278	-	-	278	-	-
$E2C$	0.4690	0.3517	0.2010	0.4690	0.3517	0.2010	0.4690	-	-

Specification of natural emissions

One key difference between FaIR v2.0 and FaIR v1.3 is the treatment of natural emissions of CH_4 and N_2O. FaIR v1.3 requires a quantity of natural emissions to be specified for these gases, which is also the case for the widely used simple climate model MAGICC (Meinshausen et al., 2011a). Figure 2 in Smith et al. (2017) illustrates the time-dependent pathway of natural emissions required to reproduce the historical Representative Concentration Pathway (RCP) concentrations when the corresponding emission timeseries (Meinshausen et al., 2011b) are run through FaIR v1.3. These natural emission timeseries vary significantly over the recent past: CH_4 drops from 209Mt in 1765 to 139Mt in 1900 then rises to its fixed future (2005 onwards) value of 191Mt, at which it is fixed following; and N_2O remains relatively constant around 11Mt before dropping sharply to its fixed future value of 9Mt around 1950. This procedure of "balancing the emissions budget" to reproduce observed historical concentrations is also utilised in MAGICC (Meinshausen et al., 2011a). This is required since the RCP database emission series were created in parellel to the concentration pathways used in CMIP5 using Integrated Assessment Models Moss et al. (2010); resulting in inconsistent emission and concentraiton data. There is little evidence for the high interdecadal trends of these natural emission pathways: Arora et al. (2018) finds the total change in natural CH_4 fluxes within CLASS-CTEM between the 1850s and 2000-2008 is +17Mt, and other studies assume that there have been no significant changes (Holmes et al., 2013; Prather et al., 2012). Due to the uncertainties associated with natural emissions of CH_4 and N_2O (Turner et al., 2019; Davidson and Kanter, 2014), we have chosen to effectively fix our natural emissions by specifying a pre-industrial concentration over which anthropogenic emissions sources increase the atmospheric concentration burden, as in the CO_2 gas cycle in all FaIR versions, and tune our gas cycle parameters to bottom-up emissions (Gütschow et al., 2016; Quéré et al., 2018) and observed concentrations Meinshausen et al. (2017) entirely independently of the RCPs. For comparison with FaIR v1.3, Figure 1 in the Supplementary Information shows the residual of emissions required to reproduce the RCP historical concentrations in FaIR v2.0 and the historical RCP emissions dataset. This is closely related to Figure 2 in Smith et al. (2017), indicating that while FaIR v2.0 and v1.3 take different approaches to natural emissions, the gas cycle models used by each are similar.

Emission-driven historical simulations

Here we run FaIR v2.0 with bottom-up emissions timeseries from the Global Carbon Project for CO_2 (Quéré et al., 2018) and PRIMAP-histTP (Gütschow et al., 2016) for CH_4 and N_2O. All other forcings are best-estimates from Forster et al. (2013). Figure 1 shows the gas concentrations as simulated in FaIR v2.0 with default parameters and uncertainties as described in both the gas cycle and thermal response parameters, plotted alongside obesrved concentrations from the CMIP6 historical dataset Meinshausen et al. (2017). Inset axes show the driving emission series used. We see that in general, FaIR v2.0 does well at matching the observed values, with the largest difference occurring for pre-1950 concentrations of N_2O. However, rather than this being a fundamental issue with the model, it is clear that the emission timeseries used is not compatible with the observed concentrations, as while concentration observations start increasing pre-1900, emissions only begin to increase around 1940. This discrepancy has occurred in other N_2O modelling studies using different methods and data sources (Saikawa et al., 2014). This is an issue of ongoing research (Tian et al., 2018), and it is possible that future work may provide a firm reason for this descrepancy, allowin us to adjust our model parameters accordingly. Crucially, the model does match the trend in observed concentrations over the recent period, where we would expect the emission estimates to be most accurate. We find that the pre-industrial lifetimes of CH_4 and N_2O are 9.05 ± 0.3 and 119.9 ± 0.2 years; pre-industrial natural emissions are $230 \pm 6 MtCH_4$ and $11.3 \pm 0.2 MtN_2O\text{-}N_2$; and present-day (2016) lifetimes are 10.1 ± 0.5 and 118.5 ± 0.2 years respectively. These quantities are within the assessed ranges found in more specific studies (Prather et al., 2012, 2015; Holmes et al., 2013; Kirschke et al., 2013; Davidson and Kanter, 2014; Arora et al., 2018).

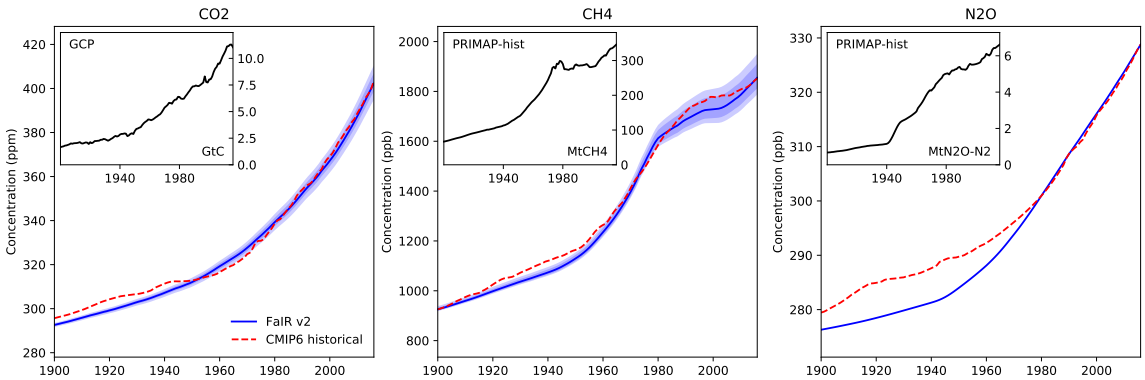

Figure 2: 1:

Other well-mixed GHGs

While here we focus on the three major GHGs, FaIR v2.0 can also be used to simulate gas cycles for the other 40 well-mixed halogenated GHGs found in the CMIP6 historical concentrations (Meinshausen et al., 2017). A figure depicting FaIR v2.0 inverse emissions from these concentrations and inverse emission estimates from a more complex atmospheric chemistry model (Cunnold et al., 1994; Rigby et al., 2011) is provided in the Supplementary Information alongside parameter values and a description of the tuning process for these gases.

3 Concentrations to effective radiative forcing

FaIR uses a simple formula to relate atmospheric gas concentrations to effective radiative forcing. This equation, below, includes logarithmic, square-root, and linear terms; motivated by the concentration-

forcing relationships in Myhre et al. (2013) of CO_2, CH_4 and N_2O, and all other well-mixed GHGs respectively.

$$F(t) = f_1 \cdot \ln\Big[\frac{C(t)}{C_0}\Big] + f_2 \cdot [C(t) - C_0] + f_3 \cdot [\sqrt{C(t)} - \sqrt{C_0}] + F_{ext}, \tag{4}$$

where the f coefficients are specified parameters, $C(t)$ is the concentration at time t and C_0 is the pre-industrial concentration of the gas species.

Selecting parameters based on Etminan et al. (2016)

FaIR v2.0 is tuned to match the simple formulae for radiative forcing of CO_2, CH_4 and N_2O given in Etminan et al. (2016). However, while Etminan et al. includes interactions between the three gases, FaIR v2.0 does not for consistency with our aim to keep the gas species independent of one another. To tune the three f parameters to Etminan, we use the CMIP6 historical concentration dataset (Meinshausen et al., 2017), and first fit them to the simple formula in Etminan et al. with interaction terms discarded. We then add on the present day value of each interaction term to the relevant f parameter (f_1 for CO_2 and f_3 for CH_4 and N_2O). Our fit parameters give an effective radiative forcing under a doubling of CO_2, $F_{2\times CO_2}$ of 3.80 Wm^{-2}.

CH_4 concentrations also indirectly affect effective radiative forcing through oxidation to stratospheric water vapour and its effect on atmospheric ozone (Noël et al., 2018; Owens et al., 1982; Myhre et al., 2013). As well as the default parameters that do not include these indirect CH_4 forcings, we provide an alternative f_2 parameter value derived from ordinary least squares regression of atmospheric CH_4 burden against best-estimate forcings of tropospheric and stratopsheric ozone, and stratospheric water vapour. The default parameters and alternative CH_4 f_2 are given below.

Table 2: Default parameter values for the concentration-forcing relationships in FaIR v2.0. An alternative CH_4 f_2 parameter value including indirect forcing effects is given in parentheses.

Parameter	CO_2	CH_4	N_2O
f_1	4.991	-0.06002	0.0009852
f_2	0.001801	-0.0001013 (0.0002873)	0.00009272
f_3	-0.02341	0.04944	0.1058

4 The thermal response model

The thermal response model is a simple linear step response model (Good et al., 2011). While previous similar models have tended to use two timescales, here we leave the number of response timescales in FaIR v2.0 general, such that if more are desired, e.g. for a faster response to volcanoes or pulse experiments as in Tsutsui (2017), the user may specify how many to use. The two equations modelling the thermal response are below.

$$\frac{\mathrm{d}S_i(t)}{\mathrm{d}t} = \frac{q_j F(t) - S_i(t)}{d_i} \tag{5}$$

$$\text{and} \quad T(t) = \sum_i^N S_i(t), \tag{6}$$

where S_i represents the temperature anomaly in box i with response timescale d_i at time t, $F(t)$ is the effective radiative forcing, and $T(t)$ is the global mean surface temperature anomaly. As in Millar et al.

(2017) and Tsutsui (2017), these equations can be solved analytically to relate q_i and d_i to the Transient Climate Response (TCR) and Equilibrium Climate Sensitivity (ECS)Collins et al. (2013) as follows:

$$\mathrm{ECS} = F_{2\times\mathrm{CO_2}} \sum_{i}^{N} q_i \tag{7}$$

$$\mathrm{TCR} = F_{2\times\mathrm{CO_2}} \sum_{i}^{N} \left\{ q_i \left(1 - \frac{d_i}{70} \left[1 - e^{-\frac{70}{d_i}} \right] \right) \right\}. \tag{8}$$

When discussing parameters for the two timescale thermal model, we quote TCR and ECS values rather than q parameters since these are the more commonly used quantities.

Selected default parameters

This thermal response model has been previously studied in detail (Geoffroy et al., 2013b,a; Gregory et al., 2015; Smith et al., 2017). Here we adopt the same default thermal response timescales as in FaIR v1.0 and v1.3 (Millar et al., 2017; Smith et al., 2017) from the CMIP5 multi-model-mean found in Geoffroy et al. (2013b). For the TCR and ECS, we adopt the central values from a lognormally distributed TCR with 5-95 percentiles of 1.0 and 2.5 (Collins et al., 2013); and a normally distributed realised warming fraction (the TCR:ECS ratio, RWF) with 5-95 percentiles of 0.45 and 0.75 (Millar et al., 2017). We specify a distribution for the RWF rather than the ECS since the RWF is shown to be more statistically independent of the TCR compared to the ECS (Millar et al., 2015). The central values are TCR = 1.58K and ECS = 2.66K, corresponding to $q_1 = 0.301$ and $q_2 = 0.399$ for our default $d_1 = 239.0$ and $d_2 = 4.10$ timescales. Following Smith et al. (2017) we use gaussian distributions truncated at $\pm 3\sigma$ for the timescales, with $[\mu\ ,\ \sigma] = [239\ ,\ 63]$ and $[4.1\ ,\ 1]$. These distributions as described above are used to generate uncertainty in the thermal response throughout this study.

Confusion arising from the thermal response of simple models

One point of contention within the recent Special Report on 1.5°C warming (IPCC, 2018, SR15) was the difference in apparent response between the two simple models FaIR v1.3 (henceforth FaIR) and MAGICC6 (MAGICC), with the FaIR response significantly below the MAGICC response in the published model outputs from the IAMC scenarios (Huppmann et al., 2018). Figures 6 and 7 below include the median total forcings and temperature responses in each model to a range of scenarios from the IMAGE 3.0.1 integrated assessment model (IAM). This shows that while the total forcings derived from emissions by each model are relatively similar, with FaIR simulating a slightly wider range (between scenarios) of forcings than MAGICC, the temperature response in FaIR is consistently lower than MAGICC, particularly notable for the high emission SSP5-Baseline scenario. This difference in response is likely due to the default parameter choice in each model, with MAGICC reseponse parameters tuned to output from CMIP3 atmosphere and oceanic general circulation models (AOGCMs) (Meinshausen et al., 2011a), while the response in FaIR (an identical thermal model to that in FaIR v2.0) was tuned to constrain modelled response to the observed temperature changes from Cowtan and Way (2014). Here we emphasize that the models themselves are not systematically biased either low or high — it is the parameters used, and how these are selected, that determines the model response. In FaIR v2.0 we have chosen to use accepted values from the literature for our thermal response parameters as above, which will have a lower default response than both MAGICC and the CMIP3, CMIP5 and CMIP6 AOGCM means, but any user can tune parameters based on what they desire FaIR v2.0 to emulate. For example, we provide FaIR v2.0 parameters tuned to a set of CMIP6 models, which should provide a thermal response more similar to MAGICC6 than the default. We argue that the high level of flexibility afforded

by the simple thermal response model in FaIR v2.0 reduces the need for multiple simple models, given its surprisingly good ability to emulate a range of more complex models Tsutsui (2017).

Emulating CMIP6 models with FaIR v2.0

Following Tsutsui (2017), we tune both the CO_2 concentration-forcing relation and the thermal response model to available output from the CMIP6 (Eyring et al., 2016) 1pctCO2 and abrupt-4×CO2 experiments. As in Tsutsui, we tune both two- and three-timescale variants of the thermal response model. We tune our three-term concentration-forcing equation to the variable logarithmic – quadratic relationship from Tsutsui, which changes functional form once the CO_2 concentration is over twice the pre-industrial value. We find that our equation is sufficient to well represent this variable relationship as shown in SI figure 3. The tuned parameters are given below for the 17 CMIP6 models with the required output available.

Table 3: Default parameter values for the CO_2 concentration-forcing parameters and thermal response parameters for emulation of CMIP6 models with FaIR v2.0. The f parameters are the same for both the two- and three-timescale variants.

CMIP6 model	Parameter timescales	f_1	f_2	f_3	d_1	d_2	d_3	q_1	q_2	q_3
BCC-CSM2-MR	2	6.415	0.005	-0.435	157.604	3.668	-	0.425	0.552	-
	3	-	-	-	170.678	7.421	0.707	0.379	0.331	0.23
BCC-ESM1	2	3.278	0.002	-0.001	193.231	4.188	-	0.48	0.591	-
	3	-	-	-	263.482	15.857	1.988	0.41	0.259	0.391
CESM2	2	14.385	0.027	-2.14	197.239	4.033	-	0.912	0.648	-
	3	-	-	-	212.316	6.079	0.942	0.941	0.475	0.201
CESM2-WACCM	2	2.584	0.004	-0.003	214.216	3.887	-	0.801	0.611	-
	3	-	-	-	219.713	4.775	0.279	0.801	0.524	0.095
CNRM-CM6-1	2	12.962	0.022	-1.732	282.876	4.571	-	0.685	0.707	-
	3	-	-	-	454.774	17.378	1.409	0.558	0.368	0.417
CNRM-ESM2-1	2	2.549	0.003	-0.002	338.245	5.905	-	0.817	0.776	-
	3	-	-	-	355.29	8.676	0.34	0.727	0.584	0.189
CanESM5	2	10.095	0.014	-1.081	231.427	6.235	-	0.788	0.769	-
	3	-	-	-	290.57	13.34	1.038	0.708	0.526	0.306
GFDL-CM4	2	7.719	0.009	-0.683	197.746	2.761	-	0.591	0.613	-
	3	-	-	-	223.729	6.994	0.98	0.592	0.301	0.347
GISS-E2-1-G	2	4.913	0.0	-0.0	334.568	2.561	-	0.308	0.481	-
	3	-	-	-	341.044	4.517	0.497	0.258	0.272	0.186
GISS-E2-1-H	2	4.633	0.001	0.0	181.44	3.693	-	0.38	0.533	-
	3	-	-	-	210.002	8.513	0.725	0.333	0.308	0.241
HadGEM3-GC31-LL	2	9.892	0.013	-1.05	203.002	6.345	-	0.779	0.739	-
	3	-	-	-	388.248	23.441	2.115	0.656	0.503	0.428
IPSL-CM6A-LR	2	13.65	0.024	-1.923	175.721	5.639	-	0.572	0.731	-
	3	-	-	-	228.387	13.099	0.868	0.481	0.48	0.31
MIROC-ES2L	2	10.883	0.015	-1.232	409.739	4.421	-	0.269	0.485	-
	3	-	-	-	591.245	9.721	0.925	0.205	0.26	0.212
MIROC6	2	3.884	0.002	0.0	315.851	3.121	-	0.282	0.48	-
	3	-	-	-	495.06	12.253	1.37	0.23	0.18	0.315
MRI-ESM2-0	2	10.552	0.016	-1.277	200.946	3.072	-	0.472	0.488	-
	3	-	-	-	202.58	4.503	0.385	0.447	0.346	0.14
SAM0-UNICON	2	5.201	0.0	0.0	260.591	3.396	-	0.478	0.57	-
	3	-	-	-	261.811	4.005	0.353	0.465	0.487	0.081
UKESM1-0-LL	2	5.283	-0.0	0.0	212.814	5.46	-	0.74	0.729	-
	3	-	-	-	323.251	17.44	1.265	0.634	0.461	0.381

At the time of writing, the required Earth System Model (ESM) output from CMIP6 for tuning the gas cycles is not available, however, this is something we aim to complete in the future, such as to be able to fully emulate the CMIP6 ESM ensemble for CO_2, CH_4 and N_2O.

5 FaIR v2.0: RCP and SSP simulations

In this section we run several standard "benchmark" tests that have been carried out by previous simple modelling groups. These include simple pulse experiments such as in Joos et al. (2013), running both the standard RCP concentrations backwards and the corresponding but not fully compatible due

to their parallel development (Moss et al., 2010) emission scenarios forwards through FaIR v2.0, and comparing simulations of the more recent SSPs (Riahi et al., 2017) from other simple models used in SR15 (Huppmann et al., 2018; IPCC, 2018) with that from FaIR v2.0.

Idealised Experiments

First, we run a series of standard pulse experiments. the model is spun up to present-day (2019) with inverse emissions derived from historical concentrations (Meinshausen et al., 2017), then concentrations of CO_2, CH_4 and N_2O are fixed at 407.9 ppm, 1867 ppb and 330.8 ppb respectively; updating and approximately replicating the experimental protocol of Joos et al. (2013). All other forcings are fixed at the 2019 value. One run is carried out with no additional emissions, and the other three have an emission pulse of 1Mt of one of the gases added in 2019. A 1Mt pulse is used since unlike in the majority of models in Joos et al. (2013), FaIR v2.0 has no internal variability, so we do not require a pulse as large as 100Gt to obatin enough signal; regardless, the results obtained are independent of the pulse size over several orders of magnitude until the equations break down and give unphysical results due to, for example, the CH_4 lifetime becoming negative as a result of the $r_T T$ term. We derive four metrics for each gas: the instantaneous airbourne fraction after 100 years – the proportion of CO_2 from the inital pulse remaining in the atmosphere; the integrated Impulse Response Function after 100 years ($iIRF_{100}$) – the integral of the instantaneous airborne fraction over the 100 years following the initial pulse; the Absolute Global Warming Potential (AGWP) – the integrated radiative forcing over a specified number of years following the pulse, normalized per kg of gas; the Global Warming Potential (GWP) after 20 and 100 years – equal to the AGWP of the gas divied by the AGWP of CO_2 over the given time period; and the initial pulse-adjustment timescale (IPT) – the time between the inital pulse and peak warming. Both CH_4 and N_2O also contribute indirectly to radiative forcing through their atmospheric chemistry, hence GWP values for direct-only forcings and full forcings, scaled as described in Myhre et al. (2013), are given. We find values comparable to the current literature (Joos et al., 2013; Ricke and Caldeira, 2014). The full CH_4 GWP is higher than previous studies (Myhre et al., 2013; Holmes et al., 2013; Etminan et al., 2016), since we have included both a longer CH_4 lifetime as in Holmes et al. (2013) and the upwards-revised radiative forcing from Etminan et al. (2016). Our calculated IPT value for CO_2 agrees well with Zickfeld and Herrington (2015); Ricke and Caldeira (2014), however we find that while the IPT does increase with the pulse size, it does not to the extend in Zickfeld and Herrington (2015); only by about 5 years for a pulse size of 1000GtC.

Table 4: Gas metric values from present-day pulse experiments.

Metric	CO_2	CH_4	N_2O
$iIRF_{100}$ (yr)	48.5 ± 2.5	11.7 ± 0.8	67.6 ± 0.1
Airborne fraction after 100 years (%)	42.8 ± 2.2	0.0 ± 0.0	42.4 ± 0.02
$AGWP_{100}$ (10^{-13} W m^{-2} yr kg^{-1})	0.842 ± 0.033	18.1 ± 0.9	259.9 ± 0.4
GWP_{100} (direct-only)	1.0 ± 0.0	21.8 ± 1.5	309 ± 12
GWP_{100} (full)	1.0 ± 0.0	36.0 ± 2.8	287 ± 11
$AGWP_{20}$ (10^{-13} W m^{-2} yr kg^{-1})	0.225 ± 0.007	15.1 ± 0.4	73.9 ± 0.0
GWP_{20} (direct-only)	1.0 ± 0.0	67.4 ± 3.0	329 ± 10
GWP_{20} (full)	1.0 ± 0.0	111.2 ± 4.9	305 ± 10
IPT (years)	11.3 [10.8 , 12.1]	6.8 [6.6 , 7.1]	16.4 [15.6 , 18.4]

We also diagnose the Transient Response to Cumulative Carbon Emissions (TCRE) within FaIR v2.0. This is the emergent linear relationship between global temperature anomalies and cumulative CO_2 emissions, attributed to a balance between the increasing airborne CO_2 fraction as atmospheric

concentrations are raised and the approximately logarithmic concentration-forcing relationship for CO_2. Here it is calculated in two ways: once following the method used in Smith et al. (2017), in which the temperature anomaly at 1000GtC was calculated when RCP8.5 was run through FaIR v1.3 (here we carry out this method using RCP4.5, 6 and 8.5, running FaIR v2.0 with concentrations and diagnosing both inverse CO_2 emissions and temperature anomalies). This method allows both the CO_2-only TCRE and effective-TCRE (when all forcing agents are included in the temperature response) to be determine. The effective-TCRE is not a strict relationship (unlike the CO_2-only TCRE), and depends considerably on the non-CO_2 forcing pathway taken. For this reason, the effective-TCRE varies considerably between RCPs. The second method used to diagnose the TCRE (CO_2-only) follows Gillett et al. (2013), in which we prescribe a 1% per year increase in CO_2 concentrations starting from pre-industrial levels, and determine the ratio of global-mean warming to cumulative CO_2 emissions at the point of CO_2 concentration doubling. The results are summarised in the table below. The result using the RCP 8.5 scenario is almost identical to FaIR v1.3, though with a larger spread more consistent with the assessed range from AR5 (Collins et al., 2013). The 1% experiment result of is consistent with a recent study (Millar and Friedlingstein, 2018) that used the historic record rather than models, though our result lowers the upper end of the TCRE distribution.

Table 5: Diagnosed TCRE in FaIR v2.0.

Method	Result
Effective-TCRE	
RCP8.5	2.06 [1.27 , 3.87]
RCP6	1.92 [1.16 , 3.58]
RCP4.5	1.96 [1.19 , 3.70]
CO_2-only TCRE	
RCP8.5	1.39 [0.89 , 2.51]
RCP6	1.41 [0.89 , 2.54]
RCP4.5	1.42 [0.90 , 2.58]
1% experiment	1.33 [0.85 , 2.16]

RCP simulations

Since the RCPs themselves are *concentration* pathways, here we focus on the results of running FaIR v2.0 with concentrations from the RCP database, as was done in the GCMs in CMIP5. We include emissions-driven runs in the Supplementary Information, but these are not comparable due to the lack of full integration between RCP concentrations and emissions as was planned in Moss et al. (2010). Figure 2 shows diagnosed emissions that are compatible with the RCP concentration series in FaIRv2.0, run with default parameters plus uncertainties as described above. Here we see the large discrepancies between FaIR v2.0 compatible emissions and the RCP database emissions for CH_4 and N_2O, while FaIRv2.0 diagnosed emissions agree well with bottom-up emission estimates to the present-day as expected, since FaIR v2.0 is tuned against a very similar historical concentration series.

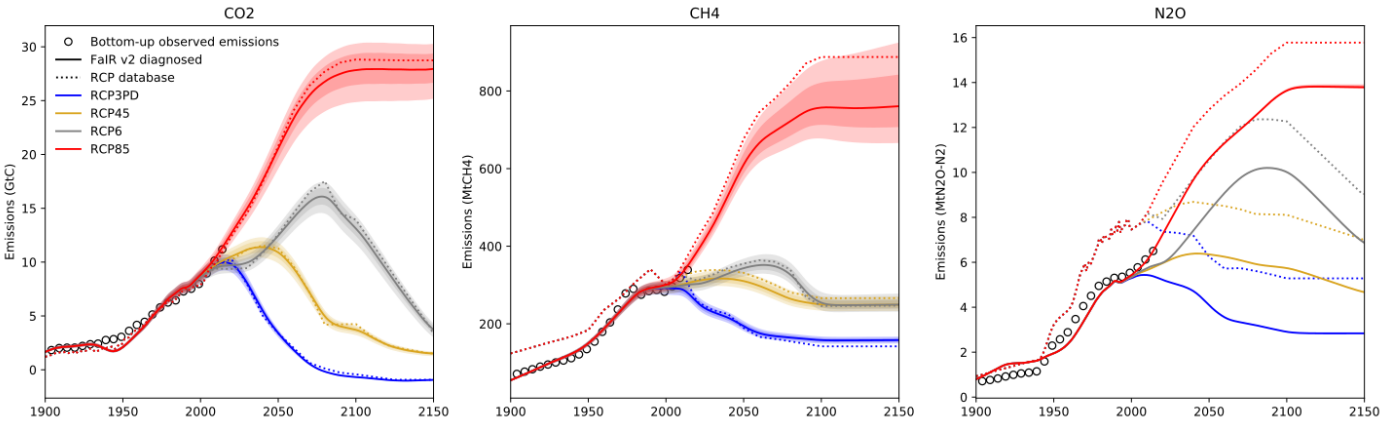

Figure 3: 2:

Figure 3 shows the corresponding radiative forcings compared to those from the RCP database. The updated simple RF formulae described in Etminan et al. (2016) increase the RF of CH_4 and CO_2, while marginally decreasing the N_2O RF.

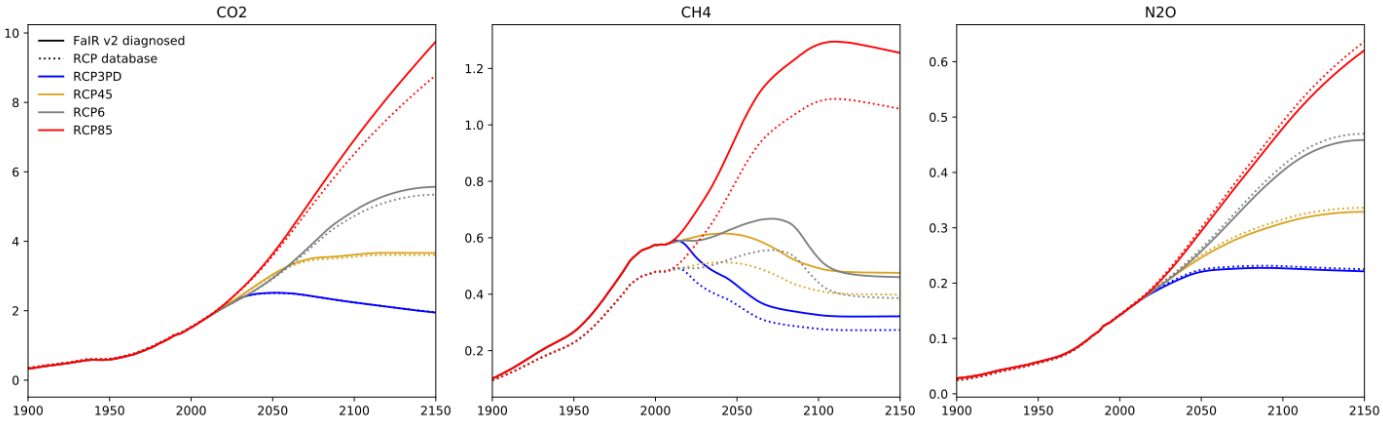

Figure 4: 3:

Figure 4 shows historical and future global mean surface temperature ranges (GMST) under the RCP scenarios diagnosed by FaIR v2.0. Also shown is the 5-year moving average of 4 observational GMST datasets (Vose et al., 2012; Cowtan and Way, 2014; Lenssen et al., 2019; Morice et al., 2011), and the CMIP5 2081:2100 gaussian mean and 5-95% ranges for RCP3PD and RCP85 (Collins et al., 2013). We see that the FaIR v2.0 diagnosed temperatures closely resemble the observed GMST series, but are lower than the CMIP5 ranges. This is due to the default climate response parameter selection as described above and is discussed fully in Richardson et al. (2016). If instead we use CMIP5 multi-model-mean two-timescale parameters (TCR, ECS, d_1 and d_2, and $F_{2\times}$) from Tsutsui (2017), we find that the resulting FaIR v2.0 temperatures much more closely resemble the CMIP5 ranges as seen in SI Figure 5, but still do not capture the full model spread for low forcing scenarios such as RCP3PD.

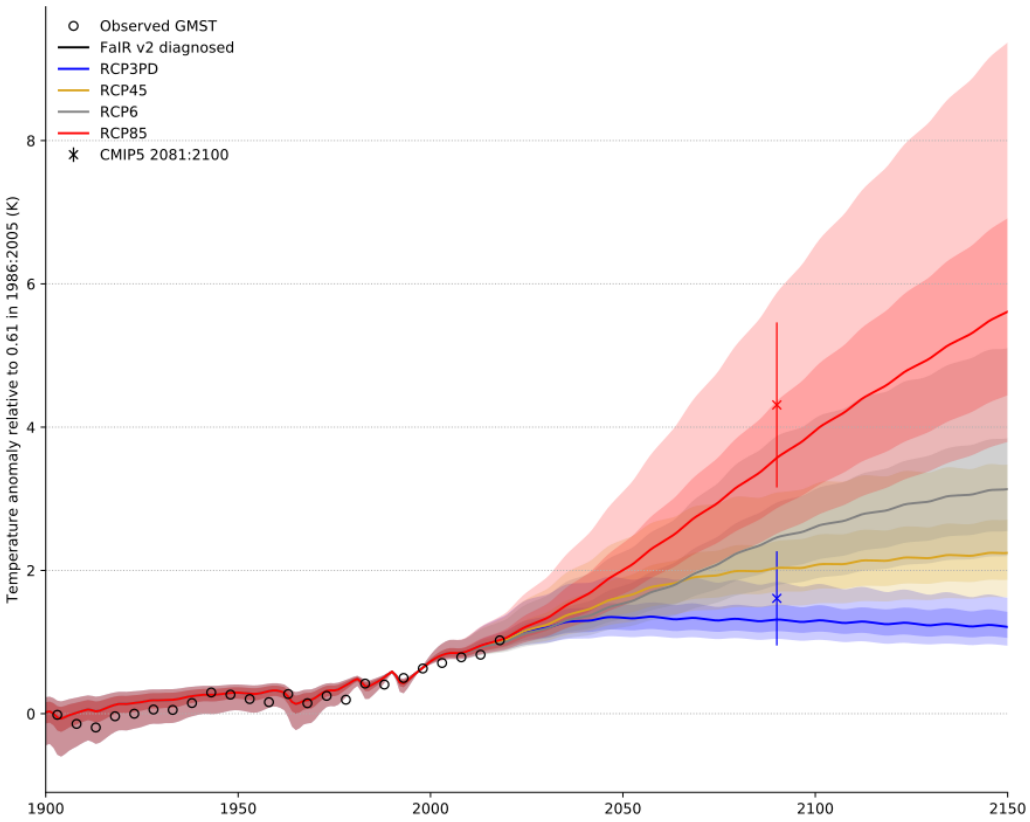

Figure 5: 4:

SSP simulations and SR15 SCM comparison

Although we include RCP simulations with FaIR v2.0 to allow comparison with the majority of the literature used, they have now been superceeded by the SSP scenarios used in SR15 (Riahi et al., 2017; IPCC, 2018). Here we explore emission-driven simulations of three of the SSPs from the IMAGE 3.0.1 integrated assessment model: SSP1-19, SSP2-45 and SSP5-Baseline. These three pathways span the range of possible future emissions and corresponding climates. Since the emissions series provided in the IAMC 1.5C database (Huppmann et al., 2018) only begin in 2005, we must harmonize these to historical series to spin up the model. We do this by diagnosing historical emissions for CO_2, CH_4 and N_2O from the CMIP6 historical concentrations (Meinshausen et al., 2017) between 1750 and 2015 in FaIR v2.0, then joining these to each SSP scenario in 2015, multiplying the SSP scenario by a linearly time dependent scaling factor – such that the SSP scenario emissions are equal to the diagnosed emissions in 2015 – that reaches a value of 1 by 2025. All other SSP forcings are harmonized identically, using best-estimate historical forcings from Forster et al. (2013). While this harmonization procedure does not exactly match the one used in the database scenarios, present-day CO_2 concentrations and total forcing is similar, and this hsould therefore be a representative comparison. The FaIR v2.0 simulated concentrations are shown in figure 5. Concentration data from other SCMs (FaIR v1.3 and MAGICC6) is only available for CO_2. We see that FaIR v2.0 simulates slightly lower CO_2 concentrations that the other SCMs, but that they generally lie within the 5-95% ranges. The small N_2O 5-95% range is due to its long lifetime and single atmospheric sink as modelled in FaIR v2.0.

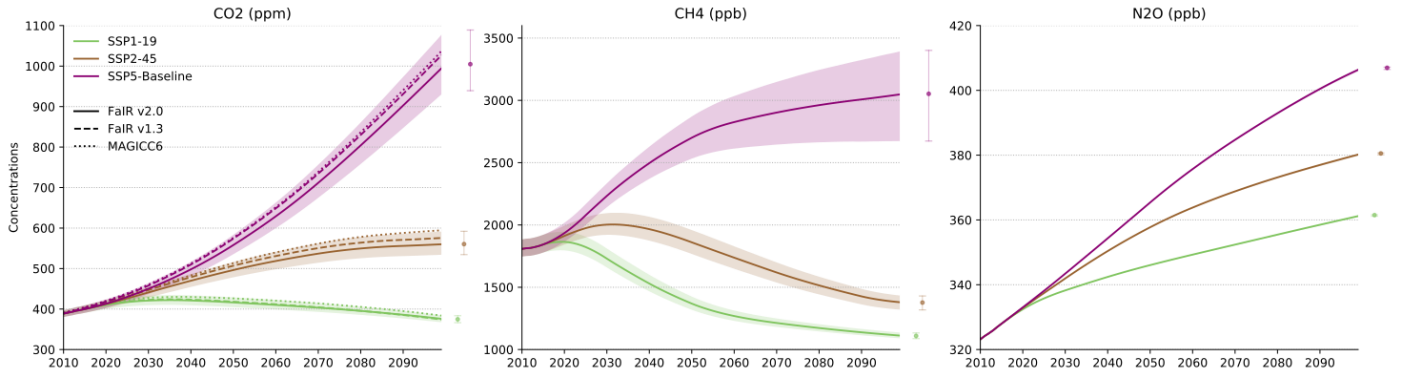

Figure 6: 5:

Median radiative forcing for each gas is available for both FaIR v1.3 and MAGICC6 in the IAMC database, so here we may do a more complete comparison between the three SCMs. Figure 6 shows that FaIR v2.0 has very similar CO_2 forcing to the other SCMs over the 21st century, lying between them for SSP5-Baseline and SSP1-19, and slightly below for SSP2-45. The other two SCMs lie within the FaIR v2.0 5-95% ranges for all time. The CH_4 forcing highlights the difference in the CH_4 concentration-forcing relationship between the models. Both FaIR v2.0 and FaIR v1.3 are based on the more recent study by Etminan et al. (2016), which revised present-day CH_4 forcing upwards by 25%, while MAGICC6 is based on Myhre et al. (2013). The difference between FaIR v2.0 and v1.3 is largely due to the different gas cycles: FaIR v2.0 has an interactive CH_4 lifetime which is longer at the present-day by default, while FaIR v1.3 keeps the CH_4 lifetime constant at 9.3 years throughout (Smith et al., 2017). FaIR v2.0 displays very similar N_2O forcing to MAGICC6, while FaIR v1.3 lies somewhat below. This discrepancy lies with the N_2O gas cycle in FaIR v1.3, since the concentration-forcing relations in FaIR v1.3 and v2.0 are extremely similar, and is likely due to its relatively low estimate of natural N_2O emissions at the present-day of 9.1 MtN_2O-N_2 (the value at which future natural emissions are fixed at). This value is taken from Prather et al. (2012), but a constant lifetime of 121 years is used, rather than the present-day lifetime estimate from that study of 131 years. This combination of low lifetime and natural emission estimate is likely the cause of the lowered future concentrations and corresponding forcing. The evolution of total forcing in each scenario is highly comparable between the models, with FaIR v2.0 lying marginally above the other two for the SSP5-Baseline scenario – due to its higher CH_4 forcing – and in between for the two lower emission scenarios.

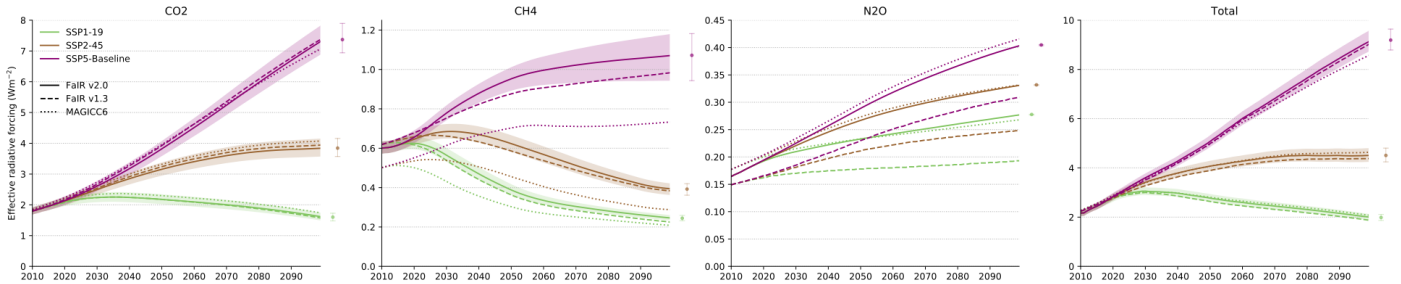

Figure 7: 6:

Finally, we compare the probabilistic temperature anomaly in each model. Figure 7 shows the median and 5-95% temperature response (min/max for CMIP6 FaIR v2.0, default FaIR v2.0 also includes the 1-σrange) in default FaIR v2.0, FaIR v1.3, MAGICC6, and FaIR v2.0 tuned to 17 CMIP6 models (two-timescale thermal response, parameters in table 3). Both FaIR v2.0 responses are relative to an anomaly of 0.61K in 1986:2005 (Kirtman et al., 2013), and the FaIR v1.3 and MAGICC6 responses are

taken directly from the database (median 2010 anomalies are 0.95, 0.86, 0.89 and 1.09 in FaIR v2.0, v1.3, MAGICC6 and CMIP6 FaIR v2.0 respectively). We see that the default FaIR v2.0 response is very similar, if marginally higher than the response of FaIR v1.3. Both versions of FaIR under default parameters have a significantly lower median response than MAGICC6, as well as a lower 5-95% spread for all scenarios. The CMIP6-tuned FaIR v2.0 has a higher response and lower spread than MAGICC6 for all scenarios, demonstrating the importance of thermal parameter choice in SCMs, since this is fundamentally the same model as default FaIR v2.0, but has a very different response.

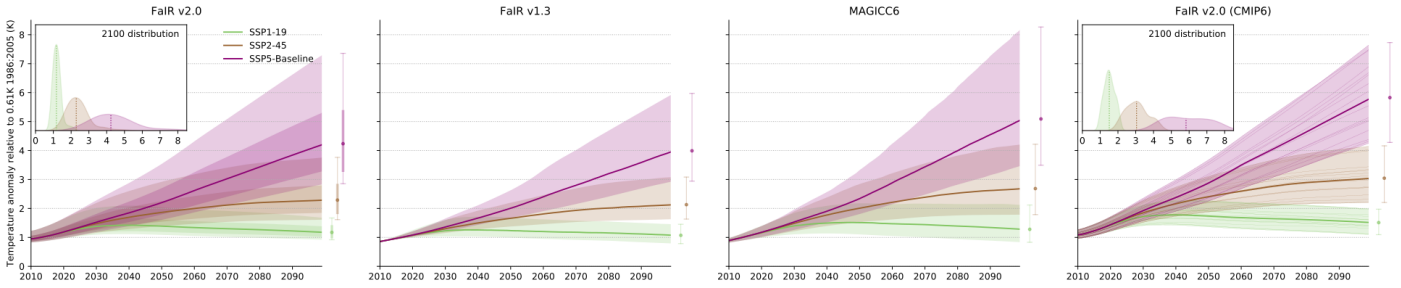

Figure 8: 7:

6 Use of FaIR v2.0

We envisage that FaIR v2.0 will largely be used for similar assessments to the current SCMs, such as providing probabilistic projections of atmospheric concentrations, radiative forcings and temperature anomalies for wide ranges of scenarios, such as was carried out to provide the SR15 scenario explorer (Huppmann et al., 2018). FaIR v2.0 could also easily be coupled to integrated assessment models (IAMs) to explore impacts of climate policy options. One advantage that FaIR v2.0 has over the other SCMs discussed here, MAGICC6 (which is already used in several IAMs) and FaIR v1.3, is its relative computational efficiency and simple equation set. Due to its parallel treatment of all the gas species, when written in a programming language designed for array operations (such as Fortran, MATLAB, or the NumPy Python module), FaIR v2.0 is extremely quick to run. For example, using its current Python code, FaIR v2.0 can compute a full emission $\rightarrow$ concentration $\rightarrow$ radiative forcing $\rightarrow$ temperature pathways for 23 $\times$ 350 year scenarios $\times$ 3 gases (plus external forcings) $\times$ 100 gas cycle parameter sets $\times$ 200 thermal response parameter sets in just over 90 seconds[1] – around 2 million years of earth-system emulation per second. This speed provides significant advantages when computing large probabilistic ensembles, or when optimizing parameters dependent on the climate system as is done in IAMs.

The six simple equations used by FaIR also provide advantages for integration into IAMs, as rather than having to integrate the original SCM code into an existing architecture, the FaIR equations set could be written up using a language and format consistent with the IAM codebase with limited effort. Their simplicity means that the model can be run in programs for analysis of tabular data, including (but not limited to) Excel. This opens up climate system exploration to a large group of potential new users who are familiar with spreadsheets, but not formal scientific programming languages. Finally, their simplicity adds considerably to the overall transparency of the model; if the model display unexpected behaviour, it is easy to determine where exactly this behaviour originates and explain it.

We suggest that the speed, simplicity and transparency of FaIR v2.0 lends it to use in undergraduate and high-school education in addition to scientific research. It can be used to explain (and demonstrate)

[1] on a laptop with 31GB RAM and an Intel(R) Core(TM) i7-8750H@2.2GHz

various aspects of both the carbon (or methane / nitrous oxide) cycle and Earth's thermal response to radiative forcing, and is simple enough to use that students could themselves carry out experiments (such as a CO_2 doubling) easily without prior experience and only basic computing skills.

The final potential use case that these authors can think of is to use FaIR v2.0 to explain differences between ESMs more simply through tuning FaIR v2.0 to emulate the ESMs and comparing differences between the tuned parameter sets to identify which aspects of the models differ most. The ability to tune FaIR v2.0 (Tsutsui, 2017; Joos et al., 2013; Millar et al., 2017) to more complex models also allows estimation of complex model response to a particular scenario or experiment without having to expend computer power to run the model itself; which itself could allow climate system uncertainties to be introduced more fully into integrated assessment studies by emulating the full CMIP6 ensemble within IAMs.

7 Conclusions

Here we present the next generation of FaIR, v2.0.

References

Allen, M. R., Frame, D. J., Huntingford, C., Jones, C. D., Lowe, J. A., Meinshausen, M., and Meinshausen, N. (2009). Warming caused by cumulative carbon emissions towards the trillionth tonne. *Nature*, 458(7242):1163–1166.

Arora, V. K., Melton, J. R., and Plummer, D. (2018). An assessment of natural methane fluxes simulated by the CLASS-CTEM model. *Biogeosciences*, 15:4683–4709.

Battle, M., Bender, M., Sowers, T., Tans, P. P., Butler, J. H., Elkins, J. W., Ellis, J. T., Conway, T., Zhang, N., Lang, P., and Clarket, A. D. (1996). Atmospheric gas concentrations over the past century measured in air from firn at the South Pole. *Nature*, 383(6597):231–235.

Butler, J. H., Battle, M., Bender, M. L., Montzka, S. A., Clarke, A. D., Saltzman, E. S., Sucher, C. M., Severinghaus, J. P., and Elkins, J. W. (1999). A record of atmospheric halocarbons during the twentieth century from polar firn air. *Nature*, 399(6738):749–755.

Collins, M., Knutti, R., Arblaster, J., Dufresne, J.-L., Fichefet, T., Friedlingstein, P., Gao, X., Gutowski, W. J., Johns, T., Krinner, G., Shongwe, M., Tebaldi, C., Weaver, A. J., and Wehner, M. (2013). Long-term Climate Change: Projections, Commitments and Irreversibility. In Stocker, T. F., Qin, D., Plattner, G.-K., Tignor, M., Allen, S. K., Boschung, J., Nauels, A., Xia, Y., Bex, V., and Midgley, P. M., editors, *Climate Change 2013: The Physical Science Basis. Contribution of Working Group I to the Fifth Assessment Report of the Intergovernmental Panel on Climate Change*, chapter 12, pages 1029–1136. Cambridge University Press, Cambridge, United Kingdom and New York, NY, USA.

Cowtan, K. and Way, R. G. (2014). Coverage bias in the HadCRUT4 temperature series and its impact on recent temperature trends. *Quarterly Journal of the Royal Meteorological Society*, 140(683):1935–1944.

Cunnold, D. M., Fraser, P. J., Weiss, R. F., Prinn, R. G., Simmonds, P. G., Miller, B. R., Alyea, F. N., and Crawford, A. J. (1994). Global trends and annual releases of CCl 3 F and CCl 2 F 2 estimated

from ALE/GAGE and other measurements from July 1978 to June 1991 . *Journal of Geophysical Research*, 99(D1):1107.

Davidson, E. A. and Kanter, D. (2014). Inventories and scenarios of nitrous oxide emissions. *Environmental Research Letters*, 9(10).

Etminan, M., Myhre, G., Highwood, E. J., and Shine, K. P. (2016). Radiative forcing of carbon dioxide, methane, and nitrous oxide: A significant revision of the methane radiative forcing. *Geophysical Research Letters*, 43(24):12,614–12,623.

Eyring, V., Bony, S., Meehl, G. A., Senior, C. A., Stevens, B., Stouffer, R. J., and Taylor, K. E. (2016). Overview of the Coupled Model Intercomparison Project Phase 6 (CMIP6) experimental design and organization. *Geoscientific Model Development*, 9(5):1937–1958.

Forster, P. M., Andrews, T., Good, P., Gregory, J. M., Jackson, L. S., and Zelinka, M. (2013). Evaluating adjusted forcing and model spread for historical and future scenarios in the CMIP5 generation of climate models. *Journal of Geophysical Research: Atmospheres*, 118(3):1139–1150.

Geoffroy, O., Saint-Martin, D., Bellon, G., Voldoire, A., Olivié, D. J. L., Tytéca, S., Geoffroy, O., Saint-Martin, D., Bellon, G., Voldoire, A., Olivié, D. J. L., and Tytéca, S. (2013a). Transient Climate Response in a Two-Layer Energy-Balance Model. Part II: Representation of the Efficacy of Deep-Ocean Heat Uptake and Validation for CMIP5 AOGCMs. *Journal of Climate*, 26(6):1859–1876.

Geoffroy, O., Saint-Martin, D., Olivié, D. J. L., Voldoire, A., Bellon, G., Tytéca, S., Geoffroy, O., Saint-Martin, D., Olivié, D. J. L., Voldoire, A., Bellon, G., and Tytéca, S. (2013b). Transient Climate Response in a Two-Layer Energy-Balance Model. Part I: Analytical Solution and Parameter Calibration Using CMIP5 AOGCM Experiments. *Journal of Climate*, 26(6):1841–1857.

Gillett, N. P., Arora, V. K., Matthews, D., Allen, M. R., Gillett, N. P., Arora, V. K., Matthews, D., and Allen, M. R. (2013). Constraining the Ratio of Global Warming to Cumulative CO ₂ Emissions Using CMIP5 Simulations*. *Journal of Climate*, 26(18):6844–6858.

Good, P., Gregory, J. M., and Lowe, J. A. (2011). A step-response simple climate model to reconstruct and interpret AOGCM projections. *Geophysical Research Letters*, 38(1):n/a–n/a.

Gregory, J. M., Andrews, T., and Good, P. (2015). The inconstancy of the transient climate response parameter under increasing CO ₂. *Philosophical Transactions of the Royal Society A: Mathematical, Physical and Engineering Sciences*, 373(2054):20140417.

Gütschow, J., Jeffery, M. L., Gieseke, R., Gebel, R., Stevens, D., Krapp, M., and Rocha, M. (2016). The PRIMAP-hist national historical emissions time series. *Earth System Science Data*, 8(2):571–603.

Haustein, K., Allen, M. R., Forster, P. M., Otto, F. E. L., Mitchell, D. M., Matthews, H. D., and Frame, D. J. (2017). A real-time Global Warming Index. *Scientific Reports*, 7(1):15417.

Holmes, C. D., Prather, M. J., Søvde, O. A., and Myhre, G. (2013). Future methane, hydroxyl, and their uncertainties: Key climate and emission parameters for future predictions. *Atmospheric Chemistry and Physics*, 13:285–302.

Huppmann, D., Kriegler, E., Krey, V., Riahi, K., Rogelj, J., Rose, S. K., Weyant, J., Bauer, N., Bertram, C., Bosetti, V., Calvin, K., Doelman, J., Drouet, L., Emmerling, J., Frank, S., Fujimori, S., Gernaat, D., Grubler, A., Guivarch, C., Haigh, M., Holz, C., Iyer, G., Kato, E., Keramidas, K., Kitous, A., Leblanc, F., Liu, J.-Y., Löffler, K., Luderer, G., Marcucci, A., McCollum, D., Mima, S., Popp, A.,

Sands, R. D., Sano, F., Strefler, J., Tsutsui, J., Van Vuuren, D., Vrontisi, Z., Wise, M., and Zhang, R. (2018). IAMC 1.5C Scenario Explorer and Data hosted by IIASA. Integrated Assessment Modeling Consortium & International Institute for Applied Systems Analysis.

IPCC (2018). *Global warming of 1.5C. An IPCC Special Report on the impacts of global warming of 1.5C above pre-industrial levels and related global greenhouse gas emission pathways, in the context of strengthening the global response to the threat of climate change,*.

Joos, F., Roth, R., Fuglestvedt, J. S., Peters, G. P., Enting, I. G., Von Bloh, W., Brovkin, V., Burke, E. J., Eby, M., Edwards, N. R., Friedrich, T., Frölicher, T. L., Halloran, P. R., Holden, P. B., Jones, C., Kleinen, T., Mackenzie, F. T., Matsumoto, K., Meinshausen, M., Plattner, G.-K., Reisinger, A., Segschneider, J., Shaffer, G., Steinacher, M., Strassmann, K., Tanaka, K., Timmermann, A., Weaver, A. J., Frölicher 11, T. L., Halloran, P. R., Holden, P. B., Jones, C., Kleinen, T., Mackenzie, F. T., Matsumoto, K., Meinshausen, M., Plattner, G.-K., Reisinger, A., Segschneider, J., Shaffer, G., Steinacher, M., Strassmann, K., Tanaka, K., Timmermann, A., and Weaver, A. J. (2013). Carbon dioxide and climate impulse response functions for the computation of greenhouse gas metrics: a multi-model analysis. *Atmos. Chem. Phys*, 13(5):2793–2825.

Kirschke, S., Bousquet, P., Ciais, P., Saunois, M., Canadell, J. G., Dlugokencky, E. J., Bergamaschi, P., Bergmann, D., Blake, D. R., Bruhwiler, L., Cameron-Smith, P., Castaldi, S., Chevallier, F., Feng, L., Fraser, A., Heimann, M., Hodson, E. L., Houweling, S., Josse, B., Fraser, P. J., Krummel, P. B., Lamarque, J. F., Langenfelds, R. L., Le Quéré, C., Naik, V., O'doherty, S., Palmer, P. I., Pison, I., Plummer, D., Poulter, B., Prinn, R. G., Rigby, M., Ringeval, B., Santini, M., Schmidt, M., Shindell, D. T., Simpson, I. J., Spahni, R., Steele, L. P., Strode, S. A., Sudo, K., Szopa, S., Van Der Werf, G. R., Voulgarakis, A., Van Weele, M., Weiss, R. F., Williams, J. E., and Zeng, G. (2013). Three decades of global methane sources and sinks.

Kirtman, B., Power, S. B., Adedoyin, J. A., Boer, G. J., Bojariu, R., Camilloni, I., Doblas-Reyes, F. J., Fiore, A. M., Kimoto, M., Meehl, G. A., Prather, M., Sarr, A., Schar, C., Sutton, R., vanOldenborgh, G. J., Vecchi, G., and Wang, H. J. (2013). Near-term Climate Change: Projections and Predictability. In Stocker, T. F., Qin, D., Plattner, G.-K., Tignor, M., Allen, S. K., Boschung, J., Nauels, A., Xia, Y., Bex, V., and Midgley, P. M., editors, *Climate Change 2013: The Physical Science Basis. Contribution of Working Group I to the Fifth Assessment Report of the Intergovernmental Panel on Climate Change*, chapter 11, pages 953–1028. Cambridge University Press, Cambridge, United Kingdom and New York, NY, USA.

Lenssen, N. J. L., Schmidt, G. A., Hansen, J. E., Menne, M. J., Persin, A., Ruedy, R., and Zyss, D. (2019). Improvements in the uncertainty model in the Goddard Institute for Space Studies Surface Temperature (GISTEMP) analysis. *Journal of Geophysical Research: Atmospheres*, page 2018JD029522.

Meinshausen, M., Raper, S. C. B., and Wigley, T. M. L. (2011a). Emulating coupled atmosphere-ocean and carbon cycle models with a simpler model, MAGICC6 Part 1: Model description and calibration. *Atmospheric Chemistry and Physics*, 11(4):1417–1456.

Meinshausen, M., Smith, S. J., Calvin, K., Daniel, J. S., Kainuma, M. L. T., Lamarque, J.-F., Matsumoto, K., Montzka, S. A., Raper, S. C. B., Riahi, K., Thomson, A., Velders, G. J. M., and van Vuuren, D. P. (2011b). The RCP greenhouse gas concentrations and their extensions from 1765 to 2300. *Climatic Change*, 109(1-2):213–241.

Meinshausen, M., Vogel, E., Nauels, A., Lorbacher, K., Meinshausen, N., Etheridge, D. M., Fraser, P. J., Montzka, S. A., Rayner, P. J., Trudinger, C. M., Krummel, P. B., Beyerle, U., Canadell, J. G.,

Daniel, J. S., Enting, I. G., Law, R. M., Lunder, C. R., O'Doherty, S., Prinn, R. G., Reimann, S., Rubino, M., Velders, G. J. M., Vollmer, M. K., Wang, R. H. J., and Weiss, R. (2017). Historical greenhouse gas concentrations for climate modelling (CMIP6). *Geoscientific Model Development*, 10(5):2057–2116.

Millar, R. J. and Friedlingstein, P. (2018). The utility of the historical record for assessing the transient climate response to cumulative emissions. *Philosophical Transactions of the Royal Society of London A: Mathematical, Physical and Engineering Sciences*, 376(2119).

Millar, R. J., Nicholls, Z. R., Friedlingstein, P., and Allen, M. R. (2017). A modified impulse-response representation of the global near-surface air temperature and atmospheric concentration response to carbon dioxide emissions. *Atmospheric Chemistry and Physics*, 17(11):7213–7228.

Millar, R. J., Otto, A., Forster, P. M., Lowe, J. A., Ingram, W. J., and Allen, M. R. (2015). Model structure in observational constraints on transient climate response. *Climatic Change*, 131(2):199–211.

Morice, C. P., Kennedy, J. J., Rayner, N. A., Jones, P. D., P., M. C., J., K. J., A., R. N., and D., J. P. (2011). Quantifying uncertainties in global and regional temperature change using an ensemble of observational estimates: The HadCRUT4 data set. *Journal of Geophysical Research: Atmospheres*, 117(D8).

Moss, R. H., Edmonds, J. A., Hibbard, K. A., Manning, M. R., Rose, S. K., Van Vuuren, D. P., Carter, T. R., Emori, S., Kainuma, M., Kram, T., Meehl, G. A., Mitchell, J. F. B., Nakicenovic, N., Riahi, K., Smith, S. J., Stouffer, R. J., Thomson, A. M., Weyant, J. P., and Wilbanks, T. J. (2010). The next generation of scenarios for climate change research and assessment. *Nature*, 463.

Myhre, G., Shindell, D., Breon, F.-M., Collins, W., Fuglestvedt, J., Huang, J., Koch, D., Lamarque, J.-F., Lee, D., Mendoza, B., Nakajima, T., Robock, A., Stephens, G., Takemura, T., and Zhang, H. (2013). Anthropogenic and Natural Radiative Forcing. In Stocker, T. F., Qin, D., Plattner, G.-K., Tignor, M., Allen, S. K., Boschung, J., Nauels, A., Xia, Y., Bex, V., and Midgley, P. M., editors, *Climate Change 2013: The Physical Science Basis. Contribution of Working Group I to the Fifth Assessment Report of the Intergovernmental Panel on Climate Change*, chapter 8, pages 659–740. Cambridge University Press, Cambridge, United Kingdom and New York, NY, USA.

Noël, S., Weigel, K., Bramstedt, K., Rozanov, A., Weber, M., Bovensmann, H., and Burrows, J. P. (2018). Water vapour and methane coupling in the stratosphere observed using SCIAMACHY solar occultation measurements. *Atmos. Chem. Phys*, 18:4463–4476.

Owens, A. J., Steed, J. M., Filkin, D. L., Miller, C., and Jesson, J. P. (1982). The Potential effects of increased methane on atmospheric ozone. *Geophysical Research Letters*, 9(9):1105–1108.

Prather, M. J., Holmes, C. D., and Hsu, J. (2012). Reactive greenhouse gas scenarios: Systematic exploration of uncertainties and the role of atmospheric chemistry. *Geophysical Research Letters*.

Prather, M. J., Hsu, J., DeLuca, N. M., Jackman, C. H., Oman, L. D., Douglass, A. R., Fleming, E. L., Strahan, S. E., Steenrod, S. D., Søvde, O. A., Isaksen, I. S. A., Froidevaux, L., and Funke, B. (2015). Measuring and modeling the lifetime of nitrous oxide including its variability. *Journal of Geophysical Research: Atmospheres*, 120(11):5693–5705.

Quéré, C., Andrew, R., Friedlingstein, P., Sitch, S., Hauck, J., Pongratz, J., Pickers, P., Ivar Korsbakken, J., Peters, G., Canadell, J., Arneth, A., Arora, V., Barbero, L., Bastos, A., Bopp, L., Ciais, P., Chini, L., Ciais, P., Doney, S., Gkritzalis, T., Goll, D., Harris, I., Haverd, V., Hoffman, F., Hoppema, M.,

Houghton, R., Hurtt, G., Ilyina, T., Jain, A., Johannessen, T., Jones, C., Kato, E., Keeling, R., Klein Goldewijk, K., Landschützer, P., Lefèvre, N., Lienert, S., Liu, Z., Lombardozzi, D., Metzl, N., Munro, D., Nabel, J., Nakaoka, S. I., Neill, C., Olsen, A., Ono, T., Patra, P., Peregon, A., Peters, W., Peylin, P., Pfeil, B., Pierrot, D., Poulter, B., Rehder, G., Resplandy, L., Robertson, E., Rocher, M., Rödenbeck, C., Schuster, U., Skjelvan, I., Séférian, R., Skjelvan, I., Steinhoff, T., Sutton, A., Tans, P., Tian, H., Tilbrook, B., Tubiello, F., Van Der Laan-Luijkx, I., Van Der Werf, G., Viovy, N., Walker, A., Wiltshire, A., Wright, R., Zaehle, S., and Zheng, B. (2018). Global Carbon Budget 2018. *Earth System Science Data*, 10(4):2141–2194.

Riahi, K., van Vuuren, D. P., Kriegler, E., Edmonds, J., O'Neill, B. C., Fujimori, S., Bauer, N., Calvin, K., Dellink, R., Fricko, O., Lutz, W., Popp, A., Cuaresma, J. C., KC, S., Leimbach, M., Jiang, L., Kram, T., Rao, S., Emmerling, J., Ebi, K., Hasegawa, T., Havlik, P., Humpenöder, F., Da Silva, L. A., Smith, S., Stehfest, E., Bosetti, V., Eom, J., Gernaat, D., Masui, T., Rogelj, J., Strefler, J., Drouet, L., Krey, V., Luderer, G., Harmsen, M., Takahashi, K., Baumstark, L., Doelman, J. C., Kainuma, M., Klimont, Z., Marangoni, G., Lotze-Campen, H., Obersteiner, M., Tabeau, A., and Tavoni, M. (2017). The Shared Socioeconomic Pathways and their energy, land use, and greenhouse gas emissions implications: An overview. *Global Environmental Change*, 42:153–168.

Richardson, M., Cowtan, K., Hawkins, E., and Stolpe, M. B. (2016). Reconciled climate response estimates from climate models and the energy budget of Earth. *Nature Climate Change*, 6(10):931–935.

Ricke, K. L. and Caldeira, K. (2014). Maximum warming occurs about one decade after a carbon dioxide emission. *Environmental Research Letters*, 9(12):124002.

Rigby, M., Ganesan, A. L., and Prinn, R. G. (2011). Deriving emissions time series from sparse atmospheric mole fractions. *Journal of Geophysical Research Atmospheres*, 116(8).

Saikawa, E., Prinn, R. G., Dlugokencky, E., Ishijima, K., Dutton, G. S., Hall, B. D., Langenfelds, R., Tohjima, Y., Machida, T., Manizza, M., Rigby, M., O'Doherty, S., Patra, P. K., Harth, C. M., Weiss, R. F., Krummel, P. B., Van Der Schoot, M., Fraser, P. J., Steele, L. P., Aoki, S., Nakazawa, T., and Elkins, J. W. (2014). Global and regional emissions estimates for N2O. *Atmospheric Chemistry and Physics*.

Saunois, M., Stavert, A. R., Poulter, B., Bousquet, P., Canadell, J. G., Jackson, R. B., Raymond, P. A., Dlugokencky, E. J., Houweling, S., Patra, P. K., Ciais, P., Arora, V. K., Bastviken, D., Bergamaschi, P., Blake, D. R., Brailsford, G., Carlson, K. M., Parker, R. J., Peng, C., Peng, S., Peters, G. P., Prigent, C., Prinn, R., Ramonet, M., Regnier, P., Riley, W. J., Rosentreter, J. A., Segers, A., Simpson, I. J., Shi, H., Smith, S. J., Steele, P. L., Thornton, B. F., Tian, H., Tohjima, Y., Tubiello, F. N., Tsuruta, A., Viovy, N., Voulgarakis, A., Weber, T. S., van Weele, M., van der Werf, G. R., Weiss, F., Worthy, D., Wunch, D., Yin, Y., Yoshida, Y., Zhang, W., Zhang, Z., Zhao, Y., Zheng, B., Zhu, Q., Zhu, Q., and Zhuang, Q. (2019). The Global Methane Budget 2000-2017 Earth System Science Data Discussions. *Earth System Science Data*.

Smith, C. J., Forster, P. M., Allen, M., Leach, N., Millar, R. J., Passerello, G. A., and Regayre, L. A. (2017). FAIR v1.1: A simple emissions-based impulse response and carbon cycle model. *Geoscientific Model Development Discussions*, (December):1–45.

Tian, H., Yang, J., Lu, C., Xu, R., Canadell, J. G., Jackson, R. B., Arneth, A., Chang, J., Chen, G., Ciais, P., Gerber, S., Ito, A., Huang, Y., Joos, F., Lienert, S., Messina, P., Olin, S., Pan, S., Peng, C., Saikawa, E., Thompson, R. L., Vuichard, N., Winiwarter, W., Zaehle, S., Zhang, B., Zhang,

K., and Zhu, Q. (2018). The global N2O model intercomparison project. *Bulletin of the American Meteorological Society*, 99(6):1231–1251.

Tsutsui, J. (2017). Quantification of temperature response to CO2 forcing in atmosphereocean general circulation models. *Climatic Change*, 140(2):287–305.

Turner, A. J., Frankenberg, C., and Kort, E. A. (2019). Interpreting contemporary trends in atmospheric methane. *Proceedings of the National Academy of Sciences*.

Vose, R. S., Arndt, D., Banzon, V. F., Easterling, D. R., Gleason, B., Huang, B., Kearns, E., Lawrimore, J. H., Menne, M. J., Peterson, T. C., Reynolds, R. W., Smith, T. M., Williams, C. N., Wuertz, D. B., Vose, R. S., Arndt, D., Banzon, V. F., Easterling, D. R., Gleason, B., Huang, B., Kearns, E., Lawrimore, J. H., Menne, M. J., Peterson, T. C., Reynolds, R. W., Smith, T. M., Jr., C. N. W., and Wuertz, D. B. (2012). NOAA's Merged LandOcean Surface Temperature Analysis. *Bulletin of the American Meteorological Society*, 93(11):1677–1685.

Zickfeld, K. and Herrington, T. (2015). The time lag between a carbon dioxide emission and maximum warming increases with the size of the emission.